Optical sensor based on two in-series birefringent optical fibers

Jonas H. Osório[1,2] and Cristiano M. B. Cordeiro[1,3]

[1]Instituto de Física "Gleb Wataghin", UNICAMP, Campinas, SP, Brazil

[2]email: jhosorio@ifi.unicamp.br

[3]email: cmbc@ifi.unicamp.br

Received 2 April 2013; accepted 10 June 2013;
posted 14 June 2013 (Doc. ID 187846); published 9 July 2013

An optical fiber sensor based on the combination of two spliced birefringent optical fiber sections is proposed in this paper. The sensor is built up in a Solc-filter-like configuration and a simple theoretical model based on Jones matrices is employed to predict experimental results. By choosing the suitable birefringent optical fibers (e.g., photonic crystal fibers, birefringent microfibers, elliptical core fibers, PANDA fibers, etc.), the sensor described herein allows for probing of two physical parameters (e.g., refractive index and temperature, hydrostatic pressure and temperature) or sensing the same parameter in two disconnected environments. In order to demonstrate the sensor performance, the system response was evaluated in a temperature-sensing measurement.

OCIS codes: (060.2310) Fiber optics; (060.2370) Fiber optics sensors; (260.1440) Birefringence; (280.6780) Temperature.

http://dx.doi.org/10.1364/AO.52.004915

1. Introduction

Optical fibers have acquired great importance in the field of sensors once they can be employed in setups which are able to probe different physical parameters with high sensitivity and high resolution. In addition, optical fiber sensors have small size, are lightweight, and also present electromagnetic immunity [1].

Several physical quantities can be sensed by the employment of optical fiber sensors, such as temperature, refractive index, pressure, curvature, strain, and electric current [1]. In order to measure those quantities, numerous techniques based in different fiber configurations have been developed. Fiber long-period and Bragg gratings [2,3], photonic crystal fibers [4], and birefringent fibers [5] are some of the technologies used to build up optical fiber sensors.

In this paper, it is reported an optical sensor setup based on two in-series birefringent optical fibers which are spliced in a Solc-filter-like configuration [6]. The setup employs an input and an output polarizer which are adjusted to obtain the desired response, as will be explained. The proposed configuration can be employed to sense different physical parameters if the suitable birefringent fibers are chosen. Moreover, it can be used to sense the same physical parameter in different environments or probe the same environment with different resolutions. In addition, with the purpose of evaluating the sensor performance, a temperature sensor for probing two disconnected environments was designed and characterized.

2. Theoretical Analysis

As discussed in the introduction, a configuration in which two birefringent optical fibers are spliced in order to obtain an optical sensor for dual parameter evaluation or dual environment monitoring was studied. A schematic diagram for the proposed setup is shown in Fig. 1.

In Fig. 1, broadband light [supercontinuum (SC) from a photonic crystal fiber] is polarized by the first polarizer (P_1), which is rotated by an angle α, and

1559-128X/13/204915-07$15.00/0

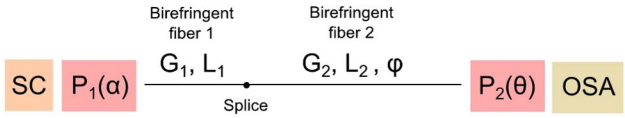

Fig. 1. Schematic diagram for the proposed sensor. SC, supercontinuum light; P_1, first polarizer; α, angle of the first polarizer; P_2, second polarizer; θ, angle of the second polarizer; L_1, length of the first fiber; L_2, length of the second fiber; G_1, group birefringence of the first fiber; G_2, group birefringence of the second fiber; φ, angle of the second fiber; OSA, optical spectrum analyzer.

then launched in the fiber so that both states of polarization of the first fiber are excited. A second polarizer (P_2), rotated by an angle θ, is placed just after the second fiber end tip, so that the waves can recombine and generate an interference pattern in the transmission spectrum [measured in an optical spectrum analyzer (OSA)]. The first birefringent fiber section has length L_1 and group birefringence G_1. The second fiber section has length L_2 and group birefringence G_2. The second fiber section is rotated by an angle φ in relation to the horizontal plane. Polarizer angles α and θ are also measured in relation to the horizontal plane.

Thus, in order to study system transmission properties, a simple theoretical model based on Jones matrices [7] was employed. The optical elements are, therefore, described by matrices and the final system response (electric field on the orthogonal directions E_x and E_y) is given by the multiplication of those matrices as shown in Eq. (1):

$$\begin{aligned}\vec{E} &= \begin{pmatrix} E_x \\ E_y \end{pmatrix} \\ &= R^{-1}(\theta)P_H R(\theta)R^{-1}(\varphi)F_2(L_2, G_2, \lambda) \\ &\quad \times R(\varphi)F_1(L_1, G_1, \lambda)R^{-1}(\alpha)P_H R(\alpha)\begin{pmatrix} 1 \\ 0 \end{pmatrix}, \end{aligned} \quad (1)$$

where

$$R(\delta) = \begin{pmatrix} \cos\delta & \sin\delta \\ -\sin\delta & \cos\delta \end{pmatrix}, \quad (2)$$

$$P_H = \begin{pmatrix} 1 & 0 \\ 0 & 0 \end{pmatrix}, \quad (3)$$

$$F_j(L_j, G_j, \lambda) = \begin{pmatrix} 1 & 0 \\ 0 & e^{i\left(\frac{2\pi L_j G_j}{\lambda}\right)} \end{pmatrix}, \quad (4)$$

and L_j and G_j are fiber length and group birefringence, respectively.

Notice that $R(\delta)$ is a rotation matrix, P_H describes a polarizer with axis parallel to the horizontal plane and F_j (L_j, G_j, λ) describes the birefringent fibers. By simplifying Eq. (1), Eq. (5) can be obtained,

$$\vec{E} = \begin{pmatrix} E_x \\ E_y \end{pmatrix} = \begin{pmatrix} \xi & \cos\theta & \cos\alpha \\ \xi & \cos\alpha & \sin\theta \end{pmatrix}, \quad (5)$$

where

$$\begin{aligned}\xi = \cos(\theta-\varphi)&\left(\cos\varphi\cos\alpha + e^{\frac{2\pi i L_1 G_1}{\lambda}}\sin\varphi\sin\alpha\right) \\ &- e^{\frac{2\pi i L_2 G_2}{\lambda}}\sin(\theta-\varphi)\left(\cos\alpha\sin\varphi - e^{\frac{2\pi i L_1 G_1}{\lambda}}\cos\varphi\sin\alpha\right).\end{aligned} \quad (6)$$

The expression for the electric fields on the orthogonal directions expressed in Eq. (5) allows calculating the system transmittance in decibels by multiplying by 10 the base-10 logarithm of the scalar product between the electric field complex conjugate Jones vector $\vec{E}^+$ and the electric field Jones vector $\vec{E}$, as it is shown in Eq. (7),

$$T = 10\log_{10}(\vec{E}^+ \cdot \vec{E}) = 10\log_{10}(\xi * \xi\cos^2\theta), \quad (7)$$

where $\xi*$ is the complex conjugate of ξ.

Theoretical model analysis revealed that it is possible to access each fiber response separately by conveniently adjusting the polarizer angles, i.e., the model predicted that it is possible to obtain separable single-fiber responses (even when the fibers are spliced by tuning the input and output polarizers regardless of the angle φ between the axes of the two fibers. The only constraint for the angle φ is $\varphi \neq m\pi/2$, where m is an integer; if $\varphi = m\pi/2$, the principal axes of the fibers will coincide and the system will act as if it was formed by only one fiber.

For accessing the first fiber response, one needs to launch light out of the fiber principal axes (by setting the angle α of the first polarizer, $\alpha = \pi/4$, for an optimized situation) and set the second polarizer at an angle θ that satisfies $\theta = \varphi$ or $\theta = \varphi + \pi/2$. For these situations, the transmittance [Eq. (7)] loses its dependence on the parameters of the second fiber (L_2 and G_2) and can be expressed as an oscillating function of the parameters of the first fiber (L_1 and G_1). Eq. (8) presents the transmittance for the situation in which $\theta = \varphi + \pi/2$:

$$T\left(\theta=\varphi+\frac{\pi}{2}\right) = 10\log_{10}\left[A(\alpha,\varphi) - B(\alpha,\varphi)\cos\left(\frac{2\pi L_1 G_1}{\lambda}\right)\right], \quad (8)$$

where

$$A(\alpha,\varphi) = \cos^2\alpha\sin^2\varphi\cos 2\varphi + \frac{\sin^2 2\alpha}{4}, \quad (9)$$

$$B(\alpha,\varphi) = \frac{\sin 2\alpha \sin 2\varphi}{4}. \quad (10)$$

For accessing the second fiber response, it is necessary to launch light at one of the first fiber principal axes and also to set the angle of the first polarizer so the electric field will be oscillating on the horizontal or vertical fiber axis $\alpha = 0$ or $\alpha = \pi/2$. When using $\alpha = \pi/2$, it is necessary to change the input electric field Jones vector in Eq. (1) $\binom{1}{0}$ by $\binom{0}{1}$; otherwise, the system response will be null. The second

polarizer is set to be at an angle θ so that $\theta \neq \varphi + \pi/2$ and $\theta \neq \varphi$; otherwise, just a single fiber axis will be probed and no modulation observed.

In this situation, the transmittance [Eq. (7)] loses its dependence on the parameters of the first fiber (L_1 and G_1) and can be expressed as an oscillating function of the parameters of the second fiber (L_2 and G_2). Equation (11) presents the transmittance for the situation in which $\alpha = 0$:

$$T(\alpha = 0) = 10 \log_{10}\left[C(\theta, \varphi) - D(\theta, \varphi) \cos\left(\frac{2\pi L_2 G_2}{\lambda}\right)\right], \tag{11}$$

where

$$C(\alpha, \varphi) = \frac{1}{2} + \frac{1}{4} \cos 2\theta + \frac{1}{4} \cos[2(\theta - 2\varphi)], \tag{12}$$

$$D(\alpha, \varphi) = \frac{1}{2} \sin 2\varphi \sin[2(\theta - \varphi)]. \tag{13}$$

Figure 2 shows theoretical plots for the transmittance of the system represented in Fig. 1 concerning the situations in which the first fiber, second fiber, and mixed responses were accessed. In order to obtain the first fiber response, the angles were set so that $\alpha = \pi/4$, $\theta = 5\pi/6$, and $\varphi = \pi/3$ (notice that $\theta = \varphi + \pi/2$). For obtaining the second fiber response, the angles were set so that $\alpha = 0$, $\theta = 7\pi/12$, and $\varphi = \pi/3$ (notice that the light was launched on the horizontal axis of the first fiber and $\theta \neq \varphi + \pi/2$). In order to exemplify a situation of mixed response, the angles were set so that $\alpha = \pi/4$, $\theta = 7\pi/12$, and $\varphi = \pi/3$. The curves were vertically shifted for better visualization.

It is worth to observe that the number of valleys (minimum points) in the individual fiber responses

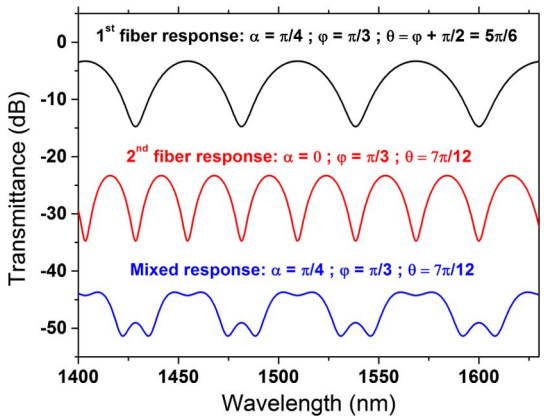

Fig. 2. Simulation of the system schematized in Fig. 1 transmittance for the situations in which the first fiber, second fiber, and mixed responses were accessed. Angles for obtaining the proposed situations: first fiber response, $\alpha = \pi/4$, $\theta = 5\pi/6$, and $\varphi = \pi/3$; second fiber response, $\alpha = 0$, $\theta = 7\pi/12$, and $\varphi = \pi/3$; mixed response, $\alpha = \pi/4$, $\theta = 7\pi/12$, and $\varphi = \pi/3$. Parameters: $L_1 = 40$ cm; $L_2 = 80$ cm; $G_1 = G_2 = 1 \times 10^{-4}$.

depends on the product between the group birefringence and the length of the fiber being measured. It can be understood, by observing Eq. (4), that the higher this product, the closer together are the wavelength values that lead to exponent values which are odd multiples of π.

The number of valleys per wavelength range in the transmission spectrum (and, therefore, the group birefringence and fiber length product) contains very important information for setting up the system reported herein. The importance arises from the fact that it is through this information that the single fiber responses are identified. For instance, if the first and the second fibers have the same group birefringence, one will need to employ fiber with different lengths; otherwise, it would be impossible to identify which fiber is being accessed.

In addition, as the individual responses of the first and second fibers can be obtained by tuning the input and output polarizer angles, we decided to evaluate the single fiber responses when their group birefringence was individually varied. This is an interesting situation since, if there is a measurable spectral change due to group birefringence variation, a sensor can be designed. The theoretical simulation concerning the situation just described is shown in Figs. 3(a) and 3(b).

Figure 3(a) shows the situation in which the first fiber response was accessed and the group birefringence of the first fiber was varied (parameters: $\alpha = \pi/4, \theta = 5\pi/6, \varphi = \pi/3, L_1 = 40$ cm, $L_2 = 80$ cm, $G_1 = G_2 = 1 \times 10^{-4}$, $\Delta G = 5 \times 10^{-7}$). Likewise, Fig. 3(b) presents the situation in which the second fiber response was accessed and the group birefringence of the second fiber was varied (parameters: $\alpha = 0, \theta = 12\pi/7, \varphi = \pi/3, L_1 = 40$ cm, $L_2 = 80$ cm, $G_1 = G_2 = 1 \times 10^{-4}$, $\Delta G = 5 \times 10^{-7}$).

One can analyze that there is a spectral shift due to the variation of the birefringence of the fiber being accessed. The referenced spectral shift can be characterized by following the position of any point in the spectrum as a function of the birefringence. The analysis proposed herein uses the position of the minimum points (valleys) to characterize the system response.

As parameters, such as refractive index, temperature, strain, and pressure can be sensed by exploring birefringence changes in birefringent optical fibers [5,6,8–11], the proposed configuration can be used to probe different physical quantities (by choosing the suitable birefringent fibers, which must be sensitive to the parameters intended to be measured). Also, it can probe the same parameter in disconnected environments (by concatenating two sections of the same birefringent fiber with different lengths).

In order to complete the design of the sensor, system cross-sensitivity was evaluated. To perform this evaluation, the birefringence of the second fiber was varied while the response of the first fiber was being measured (parameters: $\alpha = \pi/4$, $\theta = 5\pi/6$, $\varphi = \pi/3$, $L_1 = 40$ cm, $L_2 = 80$ cm, $G_1 = G_2 = 1 \times 10^{-4}$,

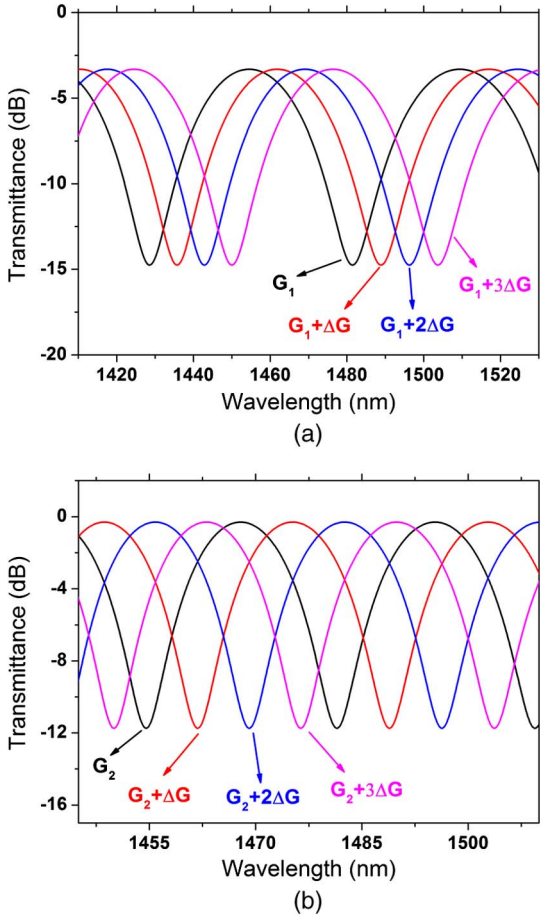

Fig. 3. (a) Simulation of the first fiber response as the birefringence of the first fiber is varied (Parameters: $\alpha = \pi/4$, $\theta = 5\pi/6$, $\varphi = \pi/3$, $L_1 = 40$ cm, $L_2 = 80$ cm, $G_1 = G_2 = 1 \times 10^{-4}$, $\Delta G = 5 \times 10^{-7}$). (b) Simulation of the second fiber response as the birefringence of the second fiber is varied (Parameters: $\alpha = 0$, $\theta = 7\pi/12$, $\varphi = \pi/3$, $L_1 = 40$ cm, $L_2 = 80$ cm, $G_1 = G_2 = 1 \times 10^{-4}$, $\Delta G = 5 \times 10^{-7}$).

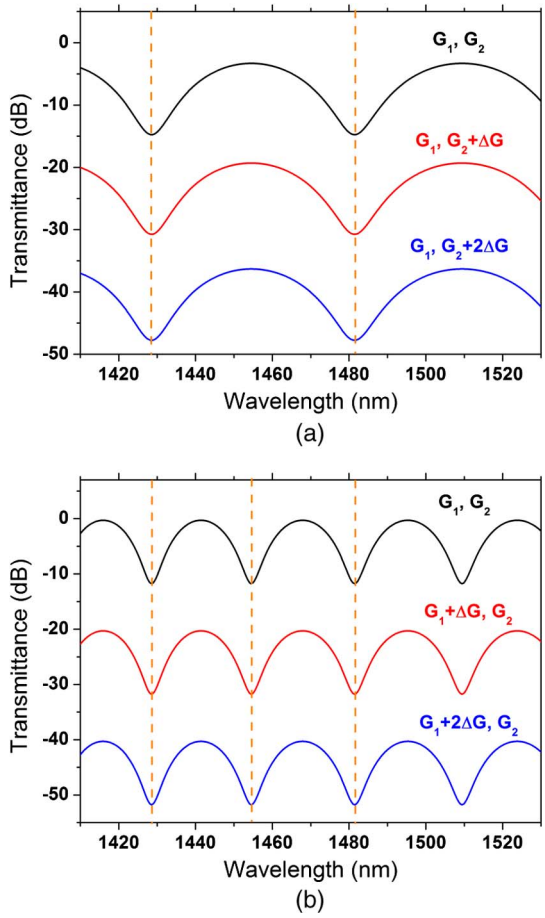

Fig. 4. (a) Simulation of the first fiber response as the birefringence of the second fiber is varied (Parameters: $\alpha = \pi/4$, $\theta = 5\pi/6$, $\varphi = \pi/3$, $L_1 = 40$ cm, $L_2 = 80$ cm, $G_1 = G_2 = 1 \times 10^{-4}$, $\Delta G = 5 \times 10^{-7}$). (b) Simulation of the second fiber response as the birefringence of the first fiber is varied (Parameters: $\alpha = 0$, $\theta = 7\pi/12$, $\varphi = \pi/3$, $L_1 = 40$ cm, $L_2 = 80$ cm, $G_1 = G_2 = 1 \times 10^{-4}$, $\Delta G = 5 \times 10^{-7}$). Vertical dashed lines helps to observe that there is no wavelength shift.

$\Delta G = 5 \times 10^{-7}$). Moreover, the situation in which the birefringence of the first fiber was varied while the response of the second fiber was being accessed was also tested (parameters: $\alpha = 0$, $\theta = 12\pi/7$, $\varphi = \pi/3$, $L_1 = 40$ cm, $L_2 = 80$ cm, $G_1 = G_2 = 1 \times 10^{-4}$, $\Delta G = 5 \times 10^{-7}$). Simulation results for those situations are presented in Figs. 4(a) and 4(b). Spectra are vertically shifted for better visualization.

It is seen in Figs. 4(a) and 4(b) that, as expected, there is no wavelength shift concerning the valley positions in the spectra. Therefore, one can observe that there is no cross sensitivity in the proposed setup, i.e., when a single fiber response is being evaluated, birefringence variations in the inactive fiber do not influence the sensor response.

Thus, the properties of the system described in Fig. 1 were theoretically analyzed and the way it can be used to sense different physical parameters or the same parameter in different environments was explained. In the next section, experimental results for the situations just analyzed will be presented and discussed.

3. System Characterization and Design of a Temperature Sensor: Experimental Approach

In order to obtain an experimental realization for the proposed system, two sections of elliptical core (e-core) optical fiber with different lengths ($L_1 = 18.1$ cm and $L_2 = 81.4$ cm) were spliced according to the configuration of Fig. 1. Figure 5 shows the single fibers and mixed responses which were obtained by tuning the input and output polarizers (spectra are vertically shifted for better visualization). It should be noted that there is no information about the orientation of the fiber ends and no information about the angle φ between the birefringent fiber sections. Thus, the polarizers are tuned by making trials.

In addition, the spectra presented in Fig. 5 allow calculating the fiber group birefringence G by using Eq. (14) where S is the valleys' wavelength spacing, λ is the wavelength, and L the length of the birefringent fiber [5]. From Fig. 5 data, one can calculate a value of 3.8×10^{-4} for the e-core fiber group

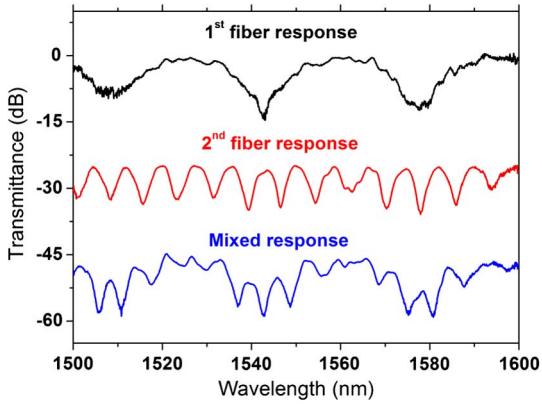

Fig. 5. Single fibers and mixed responses. Elliptical core fiber sections with different lengths were used: $L_1 = 18.1$ cm and $L_2 = 81.4$ cm.

birefringence, which is consistent to the value reported in [5], 3.85×10^{-4},

$$G = \frac{\lambda^2}{SL}. \tag{14}$$

To check the lack of cross-sensitivity, two e-core fiber sections were spliced according to the configuration presented in Fig. 1. As the e-core fiber is temperature sensitive, two situations were then evaluated: first, when the first fiber response was being measured, the second fiber section was heated; afterward, when the second fiber response was being analyzed, the first fiber section was heated. In both situations, no wavelength shifting was observed, as can be seen in Figs. 6(a) and 6(b).

In order to provide more versatility to the sensor, a configuration in which a standard single-mode fiber was spliced between the two birefringent fiber

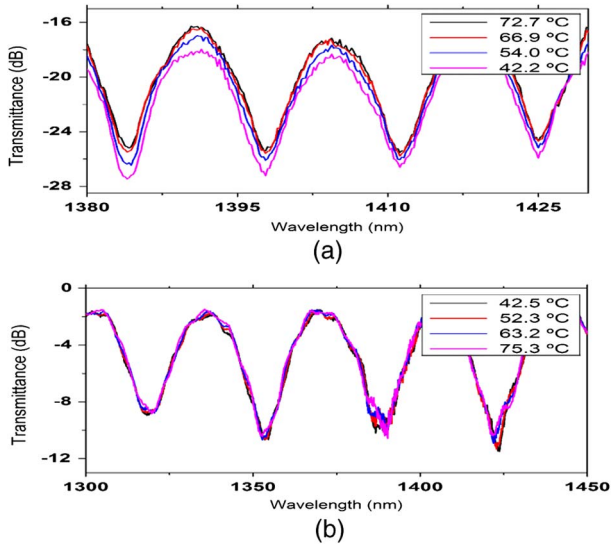

Fig. 6. Cross-sensitivity verification experiment using e-core fibers. (a) First fiber response was observed while the second fiber was heated; $L_1 = 42$ cm and $L_2 = 102.5$ cm. (b) Second fiber response was observed while the first fiber was heated; $L_1 = 73.5$ cm and $L_2 = 16$ cm.

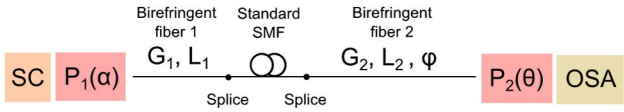

Fig. 7. Schematic diagram for the proposed sensor with a section of standard single-mode fiber placed between the birefringent fiber sections. SC, supercontinuum light; P_1, first polarizer; α, angle of the first polarizer; P_2, second polarizer; θ, angle of the second polarizer; L_1, length of the first fiber; L_2, length of the second fiber; G_1, group birefringence of the first fiber; G_2, group birefringence of the second fiber; φ, angle of the second fiber.

sections was also tested. Figure 7 shows a diagram for the setup.

Concerning the configuration presented in Fig. 7, experimental measurements showed that single-fiber responses could be obtained even with the existence of a standard telecom optical fiber section, straight or curved, between the birefringent fiber sections, as can be observed in Fig. 8 (standard telecom fiber length was 113 cm and the curvature radius had a typical value of 4 cm). Curves are vertically shifted for better visualization.

Figure 8, thus, shows that the birefringence that may be induced in the standard telecom fiber by the curvature doesn't degrade the measurement of the single-fiber responses. In [12], for instance, a birefringence of 5.3×10^{-8} is estimated for a 125 μm diameter silica fiber bent by a radius of 10 cm. By using Eq. (4), one can calculate the matrix that would describe this fiber and check that, if it is inserted in Eq. (1) the result is minimally altered; as the curvature-induced birefringence is small, the matrix that mathematically describes the standard telecom fiber section can be approximated as a unit matrix to be inserted in Eq. (1), which clearly doesn't affect this equation's original results.

To demonstrate the sensor performance, a temperature sensor for probing two disconnected environments was designed by exploring the temperature sensitivity provided by PANDA fibers. Two sections

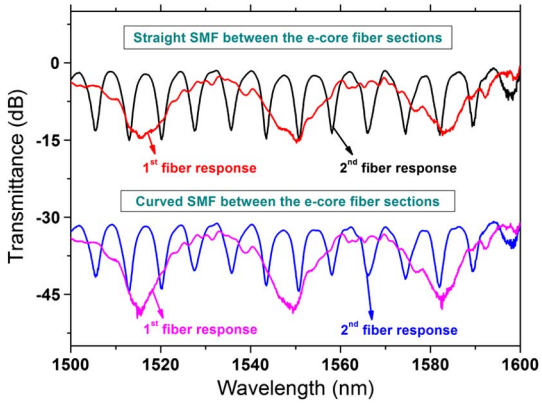

Fig. 8. Single fiber responses for the situations in which a (a) straight and (b) curved standard single-mode fiber (113 cm long) was spliced between the birefringent fiber sections (e-core fibers); $L_1 = 18.1$ cm and $L_2 = 81.4$ cm. Typical curvature radius, 4 cm.

of PANDA fiber with different lengths were then spliced to a standard telecom optical fiber according to the configuration depicted in Fig. 7 ($L_1 = 31.2$ cm; $L_2 = 91.1$ cm; Length of standard SMF fiber between PANDA fiber sections, 15.2 cm). PANDA fibers were used since they provide a temperature sensitivity which is 7 times higher than the one provided by e-core fibers [10].

The experiment is performed by first accessing the response of the first PANDA fiber section and then by heating it. Spectrum is subsequently measured as the temperature is increased and the wavelength shifting is analyzed. Similarly, the sensitivity of the second fiber is measured.

However, as the heated section of the fiber is the same for both situations (heated length $L_{\text{heat}} = 10$ cm) and the length of the PANDA fiber sections are different, one can see that different percentages of the fibers are heated. The fact of heating different percentages of the fibers implies a difference between the temperature sensitivities to be measured. To explain the difference between the temperature sensitivities, one can imagine the birefringent fiber being evaluated as divided into three parts, as shown in Fig. 9. Each division can be thought of as having $\beta_{x,i}(T,\lambda)$ and $\beta_{y,i}(T,\lambda)$ as its orthogonal mode propagation constants (dependent on temperature and wavelength) and D_i as its length.

For a certain valley position (minimum point) in the system spectrum, the phase difference between the x and y modes can be written as shown in Eq. (15):

$$\Phi = \sum_{i=1}^{i=3}[\beta_{x,i}(T,\lambda) - \beta_{y,i}(T,\lambda)]D_i = (2m+1)\pi. \quad (15)$$

Thus, with the purpose of taking into account variations in the birefringence of the fiber, one can perform a first-order Taylor expansion for the propagation constants around a temperature T_0 as shown in Eq. (16):

$$\beta(T,\lambda) = \beta(T_0,\lambda) + \frac{\partial\beta}{\partial T}dT + \frac{\partial\beta}{\partial\lambda}d\lambda. \quad (16)$$

By substituting Eq. (16) into Eq. (15) and by using the group velocity, group birefringence (G), phase birefringence (B), and propagation constants definitions, one can obtain the interferometer sensitivity to temperature (S) when a fraction of the fiber with length L_{heat} is heated,

$$S = \left(\frac{L_{\text{heat}}}{L}\right)\frac{\lambda}{G}\frac{\partial B}{\partial T}, \quad (17)$$

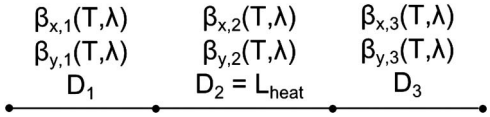

Fig. 9. Schematic diagram for analyzing sensitivity differences. The fiber is thought to be divided into three parts, each one with its mode propagation constants $\beta_{x,i}$ and $\beta_{y,I}$ and length D_i. The central part is assumed to be heated.

where L is the total length of the fiber, and $L = D_1 + D_2 + D_3$. Therefore, one can observe that the sensitivity to temperature is dependent on the fraction of the fiber that is being heated. Thus, if we consider two fibers with length L_1 and L_2 but same values for L_{heat}, B, G, and $\partial B/\partial T$ (which is the case for the experiment reported in this paper), the sensitivities S_1 and S_2 can be compared as follows:

$$\frac{S_1}{S_2} = \frac{L_2}{L_1}. \quad (18)$$

Figure 10 shows the measured spectra and the valley position plots as a function of the temperature concerning the temperature-sensing experiment. Figure 10(a) is the measurement for the situation in which the first fiber was being heated and its response evaluated. Figure 10(b) is the analogous measurement related with the second fiber. Figure 10(c) is a plot of the wavelength shift ($\Delta\lambda$) as a function of the temperature concerning the data from Figs. 10(a) and 10(b).

Figure 10 shows that the temperature from the first and the second environment could be probed. Also, it is seen that the measured sensitivities for the fiber sections were different. As explained before, the reason for this difference is that different percentages of the fiber sections were heated in the experiments (the length of fiber that was heated was the same in both situations, $L_{\text{heat}} = 10$ cm, but the fiber lengths were different: $L_1 = 31.2$ cm and $L_2 = 91.1$ cm).

By dividing the measured sensitivities ($S_1 = -0.74$ nm/°C; $S_2 = -0.25$ nm/°C), one can calculate $(S_1/S_2)_{\text{experiment}} = 2.96$. By using L_1 and L_2 values, Eq. (18) predicts $(S_1/S_2)_{\text{predicted}} = 2.92$. Thus, one can see that the experimental ratio for the temperature sensitivities is consistent with the one predicted by Eq. (18). Thus, one can analyze that a temperature sensor for dual environment probing could be obtained and characterized.

In addition, as referenced before, it should be analyzed that this Solc-like sensor configuration can probe any physical parameter to which a particular birefringent fiber is sensitive; it would be possible to sense temperature and refractive index (by using a PANDA fiber [10] and a birefringent microfiber [8,9]) or temperature and hydrostatic pressure (by using a PANDA fiber [10] and a pressure-dependent photonic crystal fiber [11]), for example.

Moreover, this sensor could be used to sense the same environment with different resolutions since the number of fringes in the spectrum (and, consequently, the FWHM of the valleys) depends on the length of the fiber in such a manner that the longer the fiber, the smaller the valley FWHM. Thus, if it is desired to perform the measurement with high resolution, the response of the longest fiber must be analyzed; if a lower resolution is required, the smallest fiber response must be monitored.

Furthermore, one should analyze that measurement dynamic range (variation range of the physical

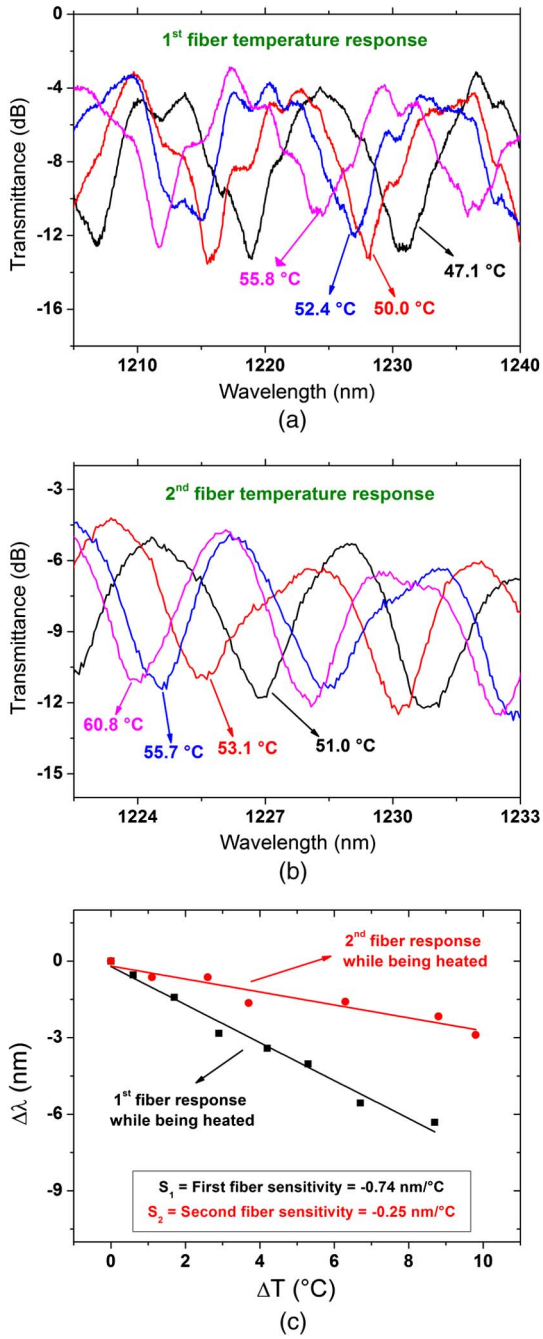

Fig. 10. (a) Measured spectra for the first PANDA fiber section while being heated. Polarizer angles: $P_1 = 350°$, $P_2 = 145°$. (b) Measured spectra for the second PANDA fiber section while being heated. Polarizer angles: $P_1 = 5°$, $P_2 = 90°$. For both experiments, PANDA fiber lengths $L_1 = 31.2$ cm; $L_2 = 91.1$ cm; Length of SMF between PANDA fiber sections, 15.2 cm; Heated length, 10 cm. (c) Wavelength shift as a function of the temperature. Temperature sensitivities S_1 = first fiber sensitivity = −0.74 nm/°C and S_2 = second fiber sensitivity = −0.25 nm/°C.

parameter to be measured, e.g., temperature interval to be evaluated) must be considered besides measurement resolution. It is important because the increase of the resolution causes the valleys to be spectrally closer. If the wavelength shift of the valleys is greater than the wavelength separation between two of them, ambiguity may occur when analyzing system response. Therefore, a high resolution measurement implies a short dynamic range to be measured, while for a measurement performed with lower resolution, a larger dynamic range can be probed.

4. Conclusion

In this paper, the development of an optical sensor which employs two sections of in-series birefringent fibers was reported. The sensor characteristics were theoretically studied by the use of Jones matrices formalism.

In order to experimentally characterize the sensor performance, a temperature sensor for dual environment probing was built up. The setup employed an input and an output polarizer which were tuned in order to access the fiber responses individually. Transmitted light was measured in an OSA and the wavelength shift of the transmission valleys due to temperature variations was monitored.

Also, it was analyzed that the reported sensor allows sensing different physical parameters if the suitable birefringent fibers are chosen. Likewise, it can be used to sense the same physical parameter in different environments if two sections of the same birefringent fiber with different lengths are used, which allows choosing the best resolution dynamic range relation for the desired measurement.

The authors would like to acknowledge Fapesp for financial support.

References

1. E. Udd and B. W. Spillman, Jr., *Fiber Optic Sensors: An Introduction for Engineers and Scientists*, 2nd ed. (Wiley, 2011).
2. S. W. James and R. P. Tatam, "Optical fibre long-period gratings sensors: characteristics and applications," Meas. Sci. Technol. **14**, R49–R61 (2003).
3. K. O. Hill and G. Meltz, "Fiber Bragg gratings technology fundamentals and overview," J. Lightwave Technol. **15**, 1263–1276 (1997).
4. P. St. J. Russel, "Photonic-crystal fibers," J. Lightwave Technol. **24**, 4729–4749 (2006).
5. O. Frazão, J. M. T. Baptista, and J. L. Santos, "Recent advances in high-birefringence fiber loop mirror sensors," Sensors **7**, 2970–2983 (2007).
6. R. H. Chu and J. J. Zou, "Transverse strain sensing based on optical Solc filter," Opt. Fiber Technol. **16**, 151–155 (2010).
7. A. Gerrard and J. M. Burch, *Introduction to Matrix Methods in Optics*, Dover Books on Physics (Wiley, 1975).
8. J. Li, L.-P. Sun, S. Gao, Z. Quan, Y.-L. Chang, Y. Ran, L. Jin, and B.-O. Guan, "Ultrasensitive refractive-index sensors based on rectangular silica microfibers," Opt. Lett. **36**, 3593–3595 (2011).
9. F. Beltrán-Mejía, J. H. Osório, C. R. Biazoli, and C. M. B. Cordeiro, "D-microfibers," Submitted to Journal of Lightwave Technology.
10. F. Zhang and J. W. Y. Lit, "Temperature and strain sensitivity measurements of high-birefringent polarization-maintaining fibers," Appl. Opt. **32**, 2213–2218 (1993).
11. H. Y. Fu, H. Y. Tam, L.-Y. Shao, X. Dong, P. K. A. Wai, C. Lu, and S. K. Khijwania, "Pressure sensor realized with polarization-maintaining photonic crystal fiber-based Sagnac interferometer," Appl. Opt. **47**, 2835–2839 (2008).
12. A. Kumar and A. Ghatak, *Polarization of Light with Applications in Optical Fibers, Tutorial Texts in Optical Engineering* (SPIE, 2011).